axioms

MDPI

Article

Precise Obstacle Avoidance Movement for Three-Wheeled Mobile Robots: A Modified Curvature Tracking Method

Xiangrong Wen [1,2] and Yusheng Zhou [2,*]

[1] Faculty of Science, Yibin University, Yibin 644000, China; 2021090009@yibinu.edu.cn
[2] School of Mathematics and Statistics, Guizhou University, Guiyang 550025, China
* Correspondence: yszhou@gzu.edu.cn

Abstract: This paper proposes a precise motion control strategy for a three-wheeled mobile robot with two driven rear wheels and one steered front wheel so that an obstacle avoidance motion task is able to be well implemented. Initially, the motion laws under nonholonomic constraints are expounded for the three-wheeled mobile robot in order to facilitate the derivation of its dynamic model. Subsequently, a prescribed target curve is converted into a speed target through the nonholonomic constraint of zero lateral speed. A modified dynamical tracking target that is aligned with the dynamic model is then developed based on the relative curvature of the prescribed curve. By applying this dynamical tracking target, path tracking precision is enhanced through appropriate selection of a yaw motion speed target, thus preventing speed errors from accumulating during relative curvature tracking. On this basis, integral sliding mode control and feedback linearization methods are adopted for designing robust controllers, enabling the accurate movement of the three-wheeled mobile robot along a given path. A theoretical analysis and simulation results corroborate the effectiveness of the proposed trajectory tracking control strategy in preventing off-target deviations, even with significant speed errors.

Keywords: nonholonomic constraint; relative curvature; three-wheeled mobile robot; dynamical tracking target; cumulative location error

MSC: 37J60; 37N35

check for updates

Citation: Wen, X.; Zhou, Y. Precise Obstacle Avoidance Movement for Three-Wheeled Mobile Robots: A Modified Curvature Tracking Method. *Axioms* **2024**, *13*, 389. https://doi.org/10.3390/axioms13060389

Academic Editors: Shengda Zeng, Stanisław Migórski and Gustavo Olague

Received: 24 April 2024
Revised: 27 May 2024
Accepted: 31 May 2024
Published: 8 June 2024

Copyright: © 2024 by the authors. Licensee MDPI, Basel, Switzerland. This article is an open access article distributed under the terms and conditions of the Creative Commons Attribution (CC BY) license (https://creativecommons.org/licenses/by/4.0/).

1. Introduction

Wheeled mobile robots, as a kind of frequently used mechanical model, are driven by actuators acting on wheels. Due to their simple structure, high maneuverability, and low energy consumption, wheeled mobile robots have garnered increasing attention in the fields of human transporters and humanoid robots [1,2]. They can be categorized based on the number of wheels, ranging from single-wheeled to multi-wheeled configurations. Among these, the three-wheeled mobile robot (TWMR for short) stands out due to its stability in the vertical direction—offering better stability compared to single or two-wheeled counterparts—and greater flexibility and smaller footprint compared to four-wheeled models [3]. These advantages make TWMRs widely applicable across various domains. For instance, the Canguro three-wheeled robot developed by Chiba University of Japan in 2008 exemplifies the practical use of TWMRs for following users and carrying items. Additionally, the advancement of autonomous driving technology for wheeled mobile robots holds promise for enhancing traffic safety, road utilization, and travel efficiency in the future. Accordingly, the most important feature for automated driving for TWMRs is the ability to avoid obstacles for safety. To achieve satisfactory obstacle avoidance performance, two steps need to be taken into account [4,5]. One is to provide a reasonable trajectory curve from the current position to a safe location, and the other is to develop an effective trajectory tracking strategy so that the TWMR can accurately track the desired

path. In general, according to the types of wheels, TWMRs are mainly categorized into three groups, including two driven wheels with one steered wheel, two driven wheels with one castor wheel, and three omnidirectional wheels [6,7]. Among these, the case of two driven wheels with one steered wheel is characterized by a simpler structure, higher load capacity, and lower control torque requirements. Despite these advantages, the complex motion laws under nonholonomic constraints have limited the extent of research on this type, making it the focus of investigation in this paper.

Trajectory tracking control is a fundamental concern for TWMRs. Current research predominantly centers on kinematic models for designing speed controllers [8,9]. Nevertheless, in practical implementations, the required speeds are usually achieved by either forces or torques. Consequently, dynamic models should be considered to devise torque controllers [10,11], which are typically implemented through current or voltage controllers. For instance, a novel three-level dynamic tracking controller has been proposed that takes into account actuators and power stage subsystems; this is more accordant with practical situations [12,13]. Moreover, actual motion tasks often necessitate TWMRs to follow a specified path, whereas dynamic models only describe the relationship between speed and control torque. To address this obstruction, it is necessary to convert the required path curve to a speed target format to ensure compatibility with the dynamic model. In this sense, the original motion issue can be transformed to a conventional tracking control problem. Taking the two-wheeled inverted pendulum as an example, a prescribed trajectory curve is transformed into the tangential motion speed and yaw motion speed targets, thereby streamlining the initial motion control design problem [14].

Furthermore, in order to design an accurate and effective controller for achieving satisfactory trajectory tracking performance, it is imperative to thoroughly elucidate the motion laws of the TWMR. In recent years, many scholars have paid extensive attention to the motion laws of two-wheeled mobile robots [15,16]. However, to the best of our knowledge, limited work has explored the holonomic and nonholonomic constraints specific to TWMRs. In particular, in some existing studies, nonholonomic constraints are often overlooked. For example, the lateral speed of a three-wheeled vehicle is sometimes treated as a degree of freedom rather than a nonholonomic constraint [17,18]. Equipping TWMRs with three omnidirectional wheels enhances their motion flexibility and significantly reduces the number of nonholonomic constraints [19,20]. Moreover, in TWMRs featuring two driven wheels and one castor wheel, the nonholonomic constraints are akin to those of two-wheeled mobile robots, as the castor wheel serves a supporting role [21,22]. However, for the case of two differentially driven wheels and one steered front wheel, the nonholonomic constraints become more intricate, thus posing challenges in deriving dynamic models and motion laws [23]. Specifically, when the steering angle of the front wheel is considered as a control variable, the final dynamic model is different from the conventional form. As a consequence, the dynamical tracking target proposed in our prior work [24] does not align with this dynamic model. This significantly heightens the complexity of control design, particularly for achieving satisfactory trajectory tracking performance.

Inspired by the above analysis, this paper proposes a modified curvature tracking method to achieve satisfactory obstacle avoidance performance for the TWMR. The main contributions lie in the following.

(i) To be more realistic, the motion laws of TWMRs are elucidated by specifically considering the steering angle of the front wheel as a control variable. Subsequently, a standardized method is proposed to derive the dynamic model by sufficiently using the obtained motion laws.

(ii) A modified dynamical tracking target that fits the dynamic model very well is proposed to resolve the accurate trajectory tracking problem of the TWMR. It is composed of two parts: a yaw motion speed target and a tangential motion speed target. The former employs a suitable smooth function to design the yaw motion speed target, reducing cumulative location errors. The latter is reliant on actual yaw motion speed and allows for continuous adjustments. Consequently, the original motion issue trans-

forms into a standard path tracking control problem, enabling TWMRs to adeptly follow desired paths by tracking the relative curvature.

The remainder of the paper is organized as following. First, a system description, kinematic model, and dynamic model are given in Section 2. Then, in Section 3, the desired trajectory is converted to a modified dynamical tracking target that matches well with the dynamic model. After that, control design for an obstacle avoidance problem is discussed in Section 4. As an application in Section 5, two numerical examples are developed to demonstrate the robustness and effectiveness of the proposed method. Finally, Section 6 draws the conclusions.

2. Modeling of the TWMR

In this section, kinematic and dynamic models are established for the TWMR. The corresponding parameters and variables of the TWMR are defined in Table 1.

Table 1. Parameters and variables of the TWMR.

Notation	Definition
T_l, T_r	Torques provided by actuators acting on the left and right rear wheels
θ_l, θ_r	Rotation angles of the left and right wheels
x, y	The coordinates of point O in the $X-Y$ plane
x_C, y_C	The coordinates of the center point C in the $X-Y$ plane
x_P, y_P	The coordinates of point P in the $X-Y$ plane
φ	Steering angle of the front wheel
θ	Heading angle of the TWMR
v	Tangential speed of the TWMR, with $v := \sqrt{\dot{x}^2+\dot{y}^2}$
M_w	Mass of the wheel
r	Radius of the wheel
M_b	Mass of the center rod
g	Gravity acceleration
a	Length of the center rod
d	Distance between the two rear wheels along the axle center
I_w	Moment of inertia of the wheel along the wheel axis direction
I_{wd}	Moment of inertia of the wheel about Z-axis through the center of the wheel
I_b	Moment of inertia of the center rod about the Z-axis through point O

2.1. System Description

Consider a TWMR comprising a steered front wheel and two differentially driven rear wheels, as depicted in Figure 1, where the two driven wheels are mounted on each side of the wheel axis. The driven torques are provided by the actuator acting on two rear wheels. In addition, in terms of the center rod PO, one end is anchored to the center of the wheel axis while the other end is flexibly connected to the steered wheel. Here, we assume that the rear wheels roll purely forward with no lateral slip for modeling the TWMR conveniently. As discussed in the introduction, the primary objective is to ensure accurate movement of the midpoint O along an identical path $\hat{\boldsymbol{r}}(t) = (\hat{x}(t), \hat{y}(t))$ while avoiding collisions with obstacles.

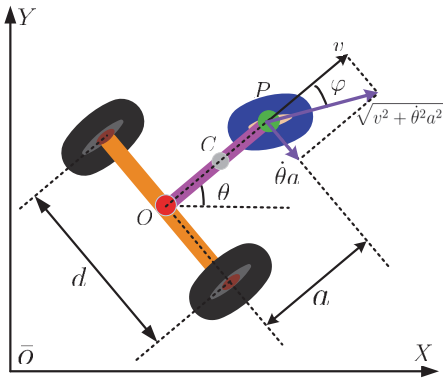


Figure 1. The model of the investigated TWMR.

2.2. Kinematic and Dynamic Models

To facilitate the establishment of the dynamic model, we introduce a generalized coordinate denoted as $\boldsymbol{q} = (x, y, \theta, \theta_l, \theta_r)^{\mathrm{T}}$ to represent the state of the TWMR.

At first, we examine the constraints imposed on the two driven rear wheels. Considering that the wheels roll purely forward without lateral slip, point O is subjected to the following two nonholonomic constraints:

$$\begin{cases} -\dot{x}\sin\theta + \dot{y}\cos\theta = 0, \\ v = \dot{x}\cos\theta + \dot{y}\sin\theta. \end{cases} \tag{1}$$

Here, the first equation indicates that the lateral speed is zero, and the second equation represents that the tangential speed at point O is the length of the tangential vector of the trajectory curve. Due to the nonholonomic constraint of zero lateral speed, point O moves along a smooth curve. We see from Equation (1) that the tangential speed at point O can be expressed as $v = \sqrt{\dot{x}^2 + \dot{y}^2}$. Thus, Equation (1) is equivalent to the following equation:

$$\begin{cases} \dot{x} = v\cos\theta, \\ \dot{y} = v\sin\theta. \end{cases} \tag{2}$$

As we know, the two driven wheels are subjected to two holonomic constraints, which are expressed as

$$\begin{cases} v = \frac{r}{2}(\dot{\theta}_l + \dot{\theta}_r), \\ \dot{\theta} = \frac{r}{d}(\dot{\theta}_l - \dot{\theta}_r). \end{cases} \tag{3}$$

Equation (3) describes the relationship between the motion speed of point O and the rotation speed of two driven wheels. Solving for $\dot{\theta}_r$ and $\dot{\theta}_l$ from Equation (3), in terms of v and $\dot{\theta}$, one has

$$\begin{cases} \dot{\theta}_l = \frac{1}{r}v + \frac{d}{2r}\dot{\theta}, \\ \dot{\theta}_r = \frac{1}{r}v - \frac{d}{2r}\dot{\theta}. \end{cases} \tag{4}$$

Now, we would like to consider the nonholonomic constraint of the steered front wheel. From Figure 1, we observe that point P represents both the front endpoint of the intermediate link and the center point of the front wheel simultaneously. For the former, it is subjected to the following nonholonomic constraint due to zero lateral velocity:

$$-\dot{x}_P\sin\varphi + \dot{y}_P\cos\varphi = 0. \tag{5}$$

From a geometric perspective, Equation (5) actually indicates that the speed of point P in the vertical direction of $\overrightarrow{OP}$ must be zero. Otherwise, if the nonholonomic constraint (5) is not satisfied, the lateral speed of point O must be nonzero, which would contradict the first nonholonomic constraint in Equation (1). For the latter, the velocity schematic of point P is shown in Figure 1. Along with Equation (5), one has

$$\frac{\dot{y}_P}{\dot{x}_P} = \tan\varphi = \frac{\dot{\theta}a}{v},$$

which yields

$$\dot{\theta} = \frac{v\tan\varphi}{a}. \tag{6}$$

Equation (6) represents a significant nonholonomic constraint that describes the relation between the steering angle φ of the front wheel and the yaw motion of the TWMR. Substituting the first equation of (2) into Equation (6), one has

$$-\dot{x}\tan\varphi + a\dot{\theta}\cos\theta = 0. \tag{7}$$

So far, two holonomic and three nonholonomic constraints of the TWMR have been clarified. Substituting Equation (3) into Equation (1), and together with Equation (7), all nonholonomic constraints are expressed as

$$\begin{cases} -\dot{x}\sin\theta + \dot{y}\cos\theta = 0, \\ \dot{x}\cos\theta + \dot{y}\sin\theta - \frac{r}{2}(\dot{\theta}_l + \dot{\theta}_r) = 0, \\ -\dot{x}\tan\varphi + a\dot{\theta}\cos\theta = 0. \end{cases} \tag{8}$$

Equation (8) can be rewritten in a matrix form as

$$\boldsymbol{F}(\boldsymbol{q})_{3\times 5}\dot{\boldsymbol{q}}_{5\times 1} = \boldsymbol{0}_{3\times 1}, \tag{9}$$

where

$$\boldsymbol{F}(\boldsymbol{q}) = \begin{bmatrix} -\sin\theta & \cos\theta & 0 & 0 & 0 \\ \cos\theta & \sin\theta & 0 & -\frac{r}{2} & -\frac{r}{2} \\ -\tan\varphi & 0 & a\cos\theta & 0 & 0 \end{bmatrix}.$$

On the other hand, from Equations (2), (4) and (6), all constraints of the TWMR are summarized by

$$\begin{cases} \dot{x} = v\cos\theta, \\ \dot{y} = v\sin\theta, \\ \dot{\theta} = \frac{v\tan\varphi}{a}, \\ \dot{\theta}_l = \frac{1}{r}v + \frac{d}{2r}\dot{\theta}, \\ \dot{\theta}_r = \frac{1}{r}v - \frac{d}{2r}\dot{\theta}. \end{cases} \tag{10}$$

Similarly, the kinematic model (10) can be further rewritten in matrix form as

$$\dot{\boldsymbol{q}}_{5\times 1} = \boldsymbol{S}(\boldsymbol{q})_{5\times 2}\boldsymbol{V}_{2\times 1}, \tag{11}$$

where

$$\boldsymbol{S}(\boldsymbol{q}) = \begin{bmatrix} \cos\theta & 0 \\ \sin\theta & 0 \\ \frac{\tan\varphi}{a} & 0 \\ \frac{1}{r} & \frac{d}{2r} \\ \frac{1}{r} & -\frac{d}{2r} \end{bmatrix}, \ \boldsymbol{V} = (v, \dot{\theta})^{\mathrm{T}}. \tag{12}$$

In fact, by multiplying $\boldsymbol{F}(\boldsymbol{q})$ by $\boldsymbol{S}(\boldsymbol{q})$, it is easy to obtain

$$\boldsymbol{F}(\boldsymbol{q})_{3\times 5} \cdot \boldsymbol{S}(\boldsymbol{q})_{5\times 2} = \boldsymbol{0}_{3\times 2}. \tag{13}$$

Now, we would like to derive the dynamic model of the TWMR. In accordance with the Euler–Lagrange equation of nonholonomic mechanical systems, the dynamic equation of the TWMR is formulated as

$$\frac{\mathrm{d}}{\mathrm{d}t}\left(\frac{\partial L}{\partial \dot{\boldsymbol{q}}}\right) - \frac{\partial L}{\partial \boldsymbol{q}} = \boldsymbol{E}(\boldsymbol{q})\boldsymbol{\tau} + \boldsymbol{F}^{\mathrm{T}}(\boldsymbol{q})\boldsymbol{\lambda}, \tag{14}$$

where $\boldsymbol{\tau}$ is the input motor-torque vector, $\boldsymbol{E}(\boldsymbol{q})$ represents the control input matrix, and $\boldsymbol{\lambda}$ denotes the so-called Lagrange multiplier. The terms $\boldsymbol{\tau}$ and $\boldsymbol{E}(\boldsymbol{q})$ are respectively given by

$$\boldsymbol{\tau} = \begin{bmatrix} \tau_l \\ \tau_r \end{bmatrix}, \quad \boldsymbol{E}(\boldsymbol{q}) = \begin{bmatrix} 0 & 0 & 0 & 0 & 1 & 0 \\ 0 & 0 & 0 & 0 & 0 & 1 \end{bmatrix}^{\mathrm{T}}. \tag{15}$$

After being further calculated in Appendix A, the dynamic Equation (14) is rewritten in a state equation form as

$$\begin{cases} \dot{v} = -\frac{Iar^2\dot{\varphi}\sin\varphi}{\Delta\cos\varphi}v + \frac{ra^2\cos^2\varphi}{\Delta}u_2, \\ \ddot{\theta} = \dot{\omega} = cu_1, \end{cases} \tag{16}$$

where $\Delta = M_1a^2r^2\cos^2\varphi + 2I_wa^2\cos^2\varphi + Ir^2\sin^2\varphi, c = \frac{r}{dI_w}$, $u_1 = T_l - T_r$, $u_2 = T_l + T_r$.

In terms of the dynamic Equation (16), u_1 is an intermediate control variable, and u_2, φ are the final control variables. Since system (16) is decoupled, u_1 can be firstly designed by the second equation. Then, according to Equation (6), φ can be calculated by

$$\dot{\theta} = \frac{v\tan\varphi}{a} = \int_0^t cu_1(\tau)\mathrm{d}\tau. \tag{17}$$

Furthermore, substituting the obtained φ into the first equation of (16), u_2 can be finally designed by common control methods. In this way, when u_1, u_2 are obtained, the desired control torques T_l and T_r for the TWMS can be derived from $T_l = \frac{1}{2}(u_1 + u_2)$ and $T_r = \frac{1}{2}(u_2 - u_1)$, respectively.

Remark 1. *In practical applications, φ, as the central control variable, determines the yaw motion of the TWMS, which is achievable through steering wheel operation. $U_2 = T_l + T_r$ provides the driving force for the TWMS by controlling the throttle. Once these two control variables are determined, the differential automatically achieves the different speeds of the left and right wheels under nonholonomic constraints. On this basis, precise motion control of the trailer is finally realized.*

3. Dynamical Trajectory Planning for an Obstacle Avoidance Problem

As shown in Figure 2, the control task of the TWMR is to follow an ideal target trajectory curve while avoiding collisions with obstacles. Assume that the shape of the planning trajectory is approximated as a cycloid curve, as can be seen by the blue line. The parametric representation of the target trajectory curve is given by

$$\hat{\boldsymbol{r}}(t) = (\hat{x}(t), \hat{y}(t)) = (\alpha[\mu t + \beta - \sin(\mu t + \beta)],\ \alpha[1 - \cos(\mu t + \beta)]), \tag{18}$$

where $t \in [0, \frac{2\pi - 2\beta}{\mu}]$, and α, β, μ are undetermined parameters of the non-standard cycloid curve that are determined by actual needs. In fact, β is a truncation parameter that affects the bending degree of the target curve. When $\beta = 0$, $\hat{\boldsymbol{r}}(t)$ represents the whole cycloid curve. The proportion of $\hat{\boldsymbol{r}}(t)$ in the cycloid curve decreases with the increment of β. The term α affects the pulling up and down of the target curve. Since the height of h is fixed, $\hat{h}$ increases with α. The term μ affects the pulling left and right of the target curve and increases with D. Note that dynamic Equation (16) only describes the relationship between the driven torques and the motion speeds. However, the actual motion task is to make the TWMR track a desired curve precisely. Thus, to match the dynamic equation, it is reasonable to transform the required path curve to a special speed target form.

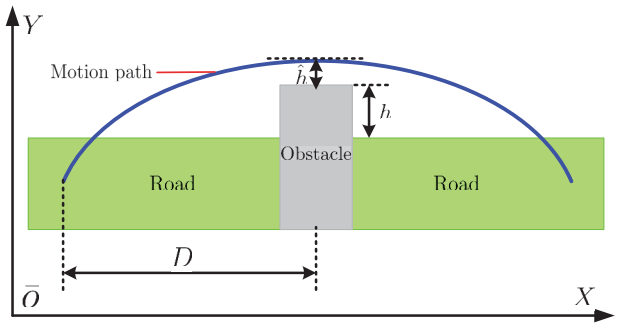


Figure 2. Schematic diagram of the obstacle avoidance motion of the TWMR.

For this purpose, assume that the smooth curve $\hat{\boldsymbol{r}}(t) = (\hat{x}(t), \hat{y}(t))$ is an actual motion trajectory of the TWMR. It follows from Equation (2) that

$$\begin{cases} \dot{\hat{x}} = \hat{v}\cos\hat{\theta} = \sqrt{\dot{\hat{x}}^2 + \dot{\hat{y}}^2}\cos\hat{\theta}, \\ \dot{\hat{y}} = \hat{v}\sin\hat{\theta} = \sqrt{\dot{\hat{x}}^2 + \dot{\hat{y}}^2}\sin\hat{\theta}, \end{cases} \tag{19}$$

where $\hat{\theta}$ represents an angle between the tangent vector of the smooth curve and the horizontal axis. Taking the derivative of both sides of Equation (19) with respect to time reads

$$\begin{cases} \ddot{\hat{x}} = \frac{1}{\hat{v}}(\dot{\hat{x}}\ddot{\hat{x}} + \dot{\hat{y}}\ddot{\hat{y}})\cos\hat{\theta} - \hat{v}\sin\hat{\theta}\dot{\hat{\theta}}, \\ \ddot{\hat{y}} = \frac{1}{\hat{v}}(\dot{\hat{x}}\ddot{\hat{x}} + \dot{\hat{y}}\ddot{\hat{y}})\sin\hat{\theta} + \hat{v}\cos\hat{\theta}\dot{\hat{\theta}}. \end{cases} \tag{20}$$

From Equations (19) and (20), we obtain

$$\dot{\hat{x}}\ddot{\hat{y}} - \ddot{\hat{x}}\dot{\hat{y}} = (\dot{\hat{x}}^2 + \dot{\hat{y}}^2)\dot{\hat{\theta}}.$$

Thus, the tangential speed and yaw motion speed of the TWMR are formulated as

$$\begin{cases} \hat{v} = \sqrt{\dot{\hat{x}}^2 + \dot{\hat{y}}^2}, \\ \dot{\hat{\theta}} = \frac{\dot{\hat{x}}\ddot{\hat{y}} - \ddot{\hat{x}}\dot{\hat{y}}}{\dot{\hat{x}}^2 + \dot{\hat{y}}^2} = k(s(t))\hat{v}, s(t) = \int_0^t \hat{v}(\tau)\mathrm{d}\tau, \end{cases} \tag{21}$$

where $k(s(t)) = \frac{\dot{\hat{x}}\ddot{\hat{y}} - \ddot{\hat{x}}\dot{\hat{y}}}{(\dot{\hat{x}}^2 + \dot{\hat{y}}^2)^{\frac{3}{2}}}$ denotes the relative curvature of the actual motion path. From Equations (19) and (21), we see that the speed $(\hat{v}, \dot{\hat{\theta}})$ uniquely determines a motion trajectory curve $\hat{\boldsymbol{r}}(t)$. However, a prescribed motion trajectory is able to be presented by different speed forms. Note that the inherent characteristic of a trajectory curve is the relative curvature. As a result, the motion trajectory $\hat{\boldsymbol{r}}(t)$ is presented in a general speed form as

$$\begin{cases} \hat{v} = \dot{\phi}(t), \\ \dot{\hat{\theta}} = k(\phi(t))\hat{v}(t). \end{cases} \tag{22}$$

Here, $\dot{\phi}(t)$ is a one-by-one arbitrary smooth function that can be designed with regard to actual needs, and $k(\phi(t))$ is the relative curvature function related to $\dot{\phi}(t)$. In an actual problem, both the initial and terminal speeds of the TWMR are zero. In this case, the tangential motion speed target is designed as

$$\dot{\phi}(t) = l\gamma^2 t\mathrm{e}^{-\gamma t}, \tag{23}$$

where l is the required motion distance, and γ is a proper parameter for the actual needs. Furthermore, the target curve (22) is described in a dynamical tracking target form as

$$\begin{cases} \hat{v} = \dot{\phi}(t), \\ \dot{\hat{\theta}} = \hat{\omega} = k(s)v(t), \ s = \int_0^t v(\tau)\mathrm{d}\tau, \end{cases} \tag{24}$$

where $v(t)$ is the actual tangential motion speed [24]. Actually, path tracking control based on Equation (24) is a curvature tracking method in essence. Hence, if the relative curvature is well tracked, the TWMR follows the ideal path accurately through dynamical tracking target (24).

In general, if Equation (24) is applied to track a smooth curve, the tangential motion speed target $\hat{v}$ should be firstly tracked. Then, the output of the actual tangential motion speed is used to construct the yaw motion speed target $\hat{\omega}$. Therefore, the control design of the tangential speed subsystem should be firstly performed; then, the yaw rotation subsystem is considered. However, according to the dynamic Equation (16) analyzed in Section 2, φ should be calculated from the intermediate control variable u_1. This implies that the yaw rotation subsystem needs to be addressed first. Thus, the designed dynamic tracking target (24) cannot align with dynamic Equation (16).

To address this issue, the dynamical tracking target (24) is further converted to a modified form as

$$\begin{cases} \dot{\hat{\theta}} = \frac{\dot{\hat{x}}\ddot{\hat{y}} - \ddot{\hat{x}}\dot{\hat{y}}}{\dot{\hat{x}}^2 + \dot{\hat{y}}^2}\dot{\phi}(t), \\ \hat{v} = \frac{\dot{\theta}}{k(s(t))}, s(t) = \int_0^t v(\tau)\mathrm{d}\tau, \end{cases} \tag{25}$$

where $\dot{\phi}(t)$ can be chosen flexibly for better tracking performance, and $\dot{\theta}$ is the actual yaw motion speed. Obviously, the modified dynamical tracking target (25) is able to match the dynamic Equation (16) very well, while retaining the merits of tracking the relative curvature. To this end, the relative curvature is calculated by

$$k(t) = \frac{-1}{4\alpha \sin\frac{\mu t+\beta}{2}}. \tag{26}$$

Moreover, the arc-length function of the trajectory curve is given by

$$\begin{aligned} s(t) &= \int_0^t \alpha\mu\sqrt{2(1-\cos(\mu\tau+\beta)}\mathrm{d}\tau \\ &= 4\alpha\cos\frac{\beta}{2} - 4\alpha\cos\frac{\mu t+\beta}{2}, \end{aligned} \tag{27}$$

and the whole length of the required path curve is expressed by

$$l = s(\frac{2\pi-2\beta}{\mu}) = 8\alpha\cos\frac{\beta}{2}. \tag{28}$$

Solving $\sin\frac{\mu t+\beta}{2}$ from (27) and substituting it into (26) gives the desired relative curvature:

$$k(s) = -\frac{1}{\sqrt{16\alpha^2 - 16\alpha^2\cos^2\frac{\beta}{2} - s^2 + 8\alpha s\cos\frac{\beta}{2}}}. \tag{29}$$

In this way, the modified dynamical tracking target (25) for the target trajectory curve (18) is eventually designed as

$$\begin{cases} \dot{\hat{\theta}} = \frac{\dot{\hat{x}}\ddot{\hat{y}} - \ddot{\hat{x}}\dot{\hat{y}}}{\dot{\hat{x}}^2+\dot{\hat{y}}^2}\dot{\phi}(t) = -\frac{\mu}{2}\dot{\phi}(t), \\ \hat{v} = -\sqrt{16\alpha^2 - 16\alpha^2\cos^2\frac{\beta}{2} - s^2 + 8\alpha\cos\frac{\beta}{2}s}\,\dot{\theta}, \end{cases} \tag{30}$$

where $s \in [0, 8\alpha\cos\frac{\beta}{2}]$. The maximum value of s represents the length of the entire trajectory curve, which is calculated by Equation (28).

4. Trajectory Tracking Control Design

In this section, we design two controllers (u_2, φ) for dynamic Equation (16) to ensure precise tracking of the target curve by the TWMR through the dynamic tracking target (30). According to the analysis in Section 3, we initially address the yaw motion subsystem to derive the intermediate control u_1 and subsequently obtain the terminal control φ through Equation (17). Next, we consider the tangential speed subsystem to design the terminal control u_2.

With regard to the yaw motion speed subsystem in the second equation of (16), we set $\boldsymbol{X} = \begin{bmatrix} x_1 \\ x_2 \end{bmatrix} = \begin{bmatrix} \theta \\ \dot{\theta} \end{bmatrix}$. Then, the yaw motion speed subsystem can be rewritten as

$$\dot{\boldsymbol{X}} = \boldsymbol{A}\boldsymbol{X} + \boldsymbol{B}u_1, \tag{31}$$

here $\boldsymbol{A} = \begin{bmatrix} 0 & 1 \\ 0 & 0 \end{bmatrix}$ and $\boldsymbol{B} = \begin{bmatrix} 0 \\ c \end{bmatrix}$. Moreover, denoting $\hat{\boldsymbol{X}} = \begin{bmatrix} \hat{x}_1 \\ \hat{x}_2 \end{bmatrix} = \begin{bmatrix} \hat{\theta} \\ \dot{\hat{\theta}} \end{bmatrix}$, $\boldsymbol{Y} = \begin{bmatrix} y_1 \\ y_2 \end{bmatrix} = \boldsymbol{X} - \hat{\boldsymbol{X}}$ and $\boldsymbol{\eta} := \boldsymbol{A}\hat{\boldsymbol{X}} - \dot{\hat{\boldsymbol{X}}}$ with $\hat{\theta} = \int_0^t \dot{\hat{\theta}}(\tau)\mathrm{d}\tau$, subsystem (31) is transformed into an error system as

$$\dot{\boldsymbol{Y}} = \boldsymbol{A}\boldsymbol{Y} + \boldsymbol{B}u_1 + \boldsymbol{\eta}. \tag{32}$$

When $\dot{\phi}(t) = l\gamma^2 t\mathrm{e}^{-\gamma t}$ is used to construct the yaw motion speed target, one can see that $\dot{\hat{\theta}}$ approaches zero as $t \to 0$, and its infinite integral is convergent. Accordingly, we reasonably

introduce the following quadratic performance index with a large weight with regard to the yaw motion speed error, described by

$$J = \frac{1}{2}\int_0^{+\infty}\left[\boldsymbol{Y}^{\mathrm{T}}\boldsymbol{Q}\boldsymbol{Y} + u_1^{\mathrm{T}}\boldsymbol{R}u_1\right]\mathrm{d}t. \tag{33}$$

In Equation (33), $\boldsymbol{R}$ and $\boldsymbol{Q}$ represent weight matrices. Due to the use of a dynamic target tracking concept, it is critical to minimize the speed tracking error (i.e., the corresponding curvature tracking error) to achieve precise tracking of the target curve. Therefore, for the parameter selection of the weight matrices discussed in Section 5, we prioritize assigning a relatively larger weight to the speed error to ensure precise tracking of the target curve.

Clearly, by employing an optimal controller u_1, the yaw motion speed error would be small via minimizing the performance index J. On the basis of LQR optimal control theory, the intermediate control variable u_1 is designed by

$$u_1 = -\boldsymbol{R}^{-1}\boldsymbol{B}^{\mathrm{T}}[\boldsymbol{P}\boldsymbol{Y} + \boldsymbol{b}]. \tag{34}$$

Here, $\boldsymbol{P}$ and $\boldsymbol{b}$ are given by

$$\begin{cases} -\boldsymbol{P}\boldsymbol{A} - \boldsymbol{A}^{\mathrm{T}}\boldsymbol{P} + \boldsymbol{P}\boldsymbol{B}\boldsymbol{R}^{-1}\boldsymbol{B}^{\mathrm{T}}\boldsymbol{P} - \boldsymbol{Q} = \boldsymbol{0}, \\ \dot{\boldsymbol{b}} = -[\boldsymbol{A} - \boldsymbol{B}\boldsymbol{R}^{-1}\boldsymbol{B}^{\mathrm{T}}\boldsymbol{P}]^{\mathrm{T}}\boldsymbol{b} - \boldsymbol{P}\boldsymbol{\eta},\ \boldsymbol{b}(+\infty) = \boldsymbol{0}. \end{cases} \tag{35}$$

The optimal controller (34) consists of two components. The first component, $-\boldsymbol{R}^{-1}\boldsymbol{B}^{\mathrm{T}}\boldsymbol{P}\boldsymbol{Y}$, is the fundamental solution to the optimal control problem, where $\boldsymbol{P}$ is determined by the first equation of Equation (35) (i.e., the Riccati equation). The second component, $-\boldsymbol{R}^{-1}\boldsymbol{B}^{\mathrm{T}}\boldsymbol{b}$, is primarily used to account for the effect of the known disturbance $\boldsymbol{\eta}$ in system (32), where $\boldsymbol{b}$ satisfies the second equation of Equation (35).

Together with Equation (17), the terminal control variable φ is formulated by

$$\varphi = \arctan\left(\frac{a\int_0^t cu_1(\tau)\mathrm{d}\tau}{v}\right). \tag{36}$$

Since the terminal control variable φ is obtained, the tangential motion speed subsystem in the first equation of (16) is taken into consideration. To address linearization errors and uncertainties, an integral sliding mode control method is introduced as follows [25,26]. We set $\bar{u} = -\frac{Iar^2\dot{\varphi}\sin\varphi}{\Delta\cos\varphi}v + \frac{ra^2\cos^2\varphi}{\Delta}u_2$ and $z = v - \hat{v}$. Then, the tangential speed subsystem is transformed into an error subsystem as

$$\dot{z} = \hat{u}_2, \tag{37}$$

where $\hat{u}_2 = \bar{u} - \dot{\hat{v}}$, and $\dot{\hat{v}} = -k(s)(4\alpha\cos\frac{\beta}{2} - s)\dot{\theta}v^2 + \frac{1}{k(s)}cu_1$. Since $\hat{u}_2$ is designed as $\hat{u}_2 = -kz$, it is easy to obtain $\bar{u} = -kz + \dot{\hat{v}}$. Then, the fundamental part of the integral sliding mode controller u_2 is obtained as

$$u_{20} = \frac{\Delta}{ra^2\cos^2\varphi}\left(-kz + \dot{\hat{v}} + \frac{Iar^2\dot{\varphi}\sin\varphi}{\Delta\cos\varphi}(z + \hat{v})\right). \tag{38}$$

Furthermore, to achieve satisfactory obstacle avoidance performance, the tracking target $\hat{v}$ is chosen as the integral sliding mode manifold $F(\hat{v}(t)) = 0$, where the sliding mode function is expressed by

$$F(v(t)) := G[v(t) - v(0)] - G\int_0^t \dot{\hat{v}}(\tau)\mathrm{d}\tau, \tag{39}$$

with $G > 0$ being an appropriate parameter. In this case, the switching control part of u_2 can be constructed by

$$u_{21} = -G^{-1}(\varepsilon + GE \mid \hat{v} - v \mid)\cdot \mathrm{sgn}(F(v(t))), \tag{40}$$

where ε is a switching control parameter, and E is the maximum energy limit of the whole of the uncertainties. As a consequence, the robust controller u_2 is finally designed by

$$u_2 = u_{20} + u_{21}. \tag{41}$$

In summary, from Equations (36) and (41), the desired controllers (φ, u_2) are eventually designted as

$$\begin{cases} \varphi = & \arctan(-\frac{ac}{v}\int_0^t \boldsymbol{R}^{-1}\boldsymbol{B}^{\mathrm{T}}[\boldsymbol{P}(\tau)\boldsymbol{Y}(\tau) + \boldsymbol{b}(\tau)]\mathrm{d}\tau), \\ u_2 = & \frac{\Delta}{ra^2\cos^2\varphi}(-kz + \dot{\hat{v}} + \frac{Iar^2\dot{\varphi}\sin\varphi}{\Delta\cos\varphi}(z + \hat{v})) - G^{-1}(\varepsilon + GE \mid \hat{v} - v \mid) \cdot \mathrm{sgn}(F(v)). \end{cases} \tag{42}$$

In light of the above analyses, the detailed control design process is as follows in Table 2:

Table 2. The control Design Process of the TWMR.

Step	Process
Step 1.	Design an appropriate target trajectory curve $\hat{\boldsymbol{r}}(t)$ based on the obstacle avoidance motion task.
Step 2.	Convert the target trajectory curve $\hat{\boldsymbol{r}}(t)$ into the dynamic speed target form (30).
Step 3.	Consider the yaw rotation subsystem in the dynamic equation, design an intermediate variable controller u_1 based on the designed yaw rotation speed target, and obtain the steering angle controller φ from Equation (17).
Step 4.	Substitute φ into the forward speed subsystem and design the torque controller u_2 in conjunction with the forward speed target, which includes the relative curvature of the desired trajectory.
Step 5.	Substitute Equation (42) into the dynamic equation for numerical simulation to verify the effectiveness and robustness of the designed controllers.

5. Simulation Results

In this section, we present two groups of simulations to demonstrate the robustness and effectiveness of the proposed tracking control strategy. First, we perform a comparison of the trajectory tracking performance between dynamical and statical tracking targets. After that, we report the trajectory tracking precision of the proposed method when subjected to unstable speed error subsystems.

For numerical simulations, the relevant parameters and initial values of the TWMR are configured as $M_B = 3$ kg, $M_w = 2$ kg, $I_w = 0.01$ kg m^2, $I_B = 0.16$ kg m^2, $I_{wd} = 0.005$ kg m^2, $a = 0.4$ m, $r = 0.1$ m, $d = 0.2$ m, $\mu = 1, g = 9.8$ m/s^2, $D = 10$ m, $h = 5$ m, $\hat{h} = 1$ m, $\boldsymbol{R} = 1$, $\boldsymbol{Q} = \mathrm{diag}(1, 100)$. Thus, the dynamic Equation (16) is expressed as

$$\begin{cases} \dot{v} = -\frac{10.8\dot{\varphi}\tan\varphi}{37\cos^2\varphi+27}v + \frac{53.33\cos^2\varphi}{37\cos^2\varphi+27}u_2, \\ \ddot{\theta} = 50u_1. \end{cases} \tag{43}$$

Since the initial speed of the dynamic tracking target is zero, it would be better to stop the three-wheeled mobile robot before performing the motion control task. Therefore, we can take the initial conditions as $\theta(0) = 1.3147$, $v(0) = 0$, and $\dot{\theta}(0) = 0$.

According to the geometric relationship in Figure 2, the parameters α and β of the target curve (18) are determined by

$$\begin{cases} \alpha\pi - \alpha(\beta - \sin\beta) = D, \\ 2\alpha - \alpha(1 - \cos\beta) = h + \hat{h}, \end{cases} \tag{44}$$

where $\hat{h}$ is the safety margin. Solving the above equations gives

$$\begin{cases} \alpha = 3.2056, \\ \beta = 0.5121. \end{cases} \tag{45}$$

Thus, the target trajectory curve (18) is approximately given by

$$\hat{\boldsymbol{r}}(t) = (3.2056 \cdot [t + 0.5121 - \sin(t + 0.5121)],\ 3.2056 \cdot [1 - \cos(t + 0.5121)]). \tag{46}$$

5.1. A Simulation Comparison between the Dynamical and the Statical Tracking Targets

We first suppose that the yaw motion speed error subsystem is affected by an uncertain factor $\boldsymbol{d}_1 = (5y_1, 5y_2)^{\mathrm{T}}$ related to the error state, and (32) becomes

$$\dot{\boldsymbol{Y}} = \boldsymbol{A}\boldsymbol{Y} + \boldsymbol{B}u_1 + \boldsymbol{\eta} + \boldsymbol{d}_1. \tag{47}$$

Meanwhile, the tangential motion speed error subsystem is assumed to be affected by an uncertain factor $d_2 = 0.1\sin t + 2z(t)$. After that, the corresponding tangential motion speed error subsystem can be expressed as

$$\dot{z} = \hat{u}_2 + d_2. \tag{48}$$

For the switching control part u_{21}, let $G = 1, \varepsilon = 0.1, E = 0.2$ and $k = 600$. With these preparations, all the quantities required for φ and u_2 are available on hand.

According to Equation (30), the modified dynamical tracking target of the target trajectory curve (46) is designed by

$$\begin{cases} \dot{\hat{\theta}} = -\frac{3}{4}t\mathrm{e}^{-\frac{1}{2}t}, \\ \hat{v} = -\sqrt{10.5476 - s^2 + 24.8089s}\,\dot{\theta}, \end{cases} \quad s \in [0, 24.8089]. \tag{49}$$

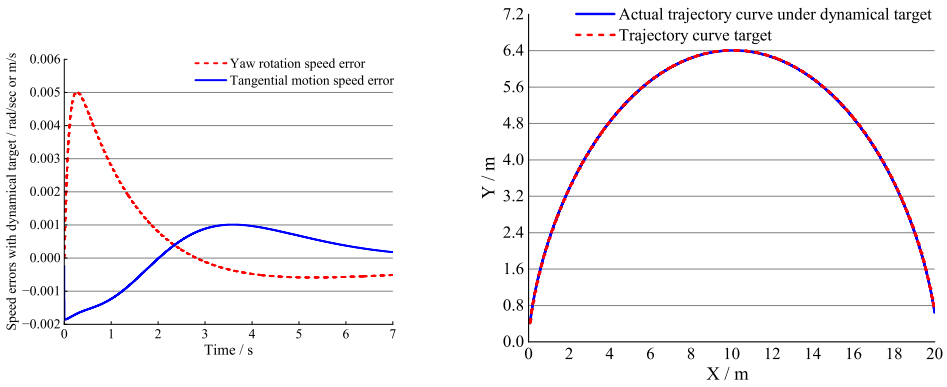
where $s = \int_0^t v(\tau)\mathrm{d}\tau$. Meanwhile, the statical tracking target (21) is expressed by

$$\begin{cases} \hat{v} = 2\alpha\sin\frac{t+\beta}{2}, \\ \dot{\hat{\theta}} = k(t)\hat{v}(t) = -\frac{1}{2}, \end{cases} \quad t \in [0, 2\pi - 2\beta]. \tag{50}$$

If (50) is adopted to design the controller (42), the initial speed error is non-zero and is described as

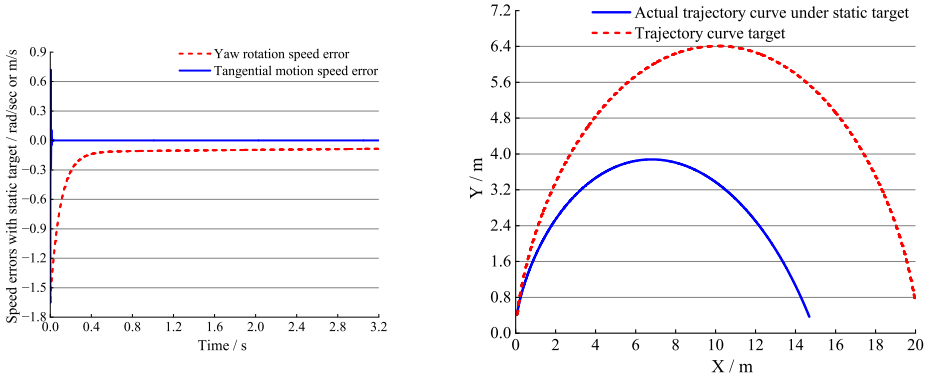
$$\begin{cases} v(0) - \hat{v}(0) = -2\alpha\sin\frac{\beta}{2} = -1.6239, \\ \dot{\theta}(0) - \dot{\hat{\theta}}(0) = \frac{1}{2}. \end{cases} . \tag{51}$$

As shown in Figure 3a, the tangential motion and yaw motion speed errors are sufficiently small when employing such a dynamic tracking target. This results in minimal accumulative location errors for the TWMR. Consequently, the actual trajectory nearly coincides with the prescribed path, as depicted in Figure 3b. However, as observed in Figure 4a, the initial speed error is significant, and the accumulative location errors increase when using the static tracking target. Correspondingly, as shown in Figure 4b, the actual trajectory deviates significantly from the target trajectory curve.



(**a**) (**b**)

Figure 3. Actual motion speed errors and motion trajectory of the TWMR via the dynamical tracking target. (**a**) Actual motion speed errors of the TWMR; (**b**) actual motion trajectory curve of the TWMR.



(**a**) (**b**)

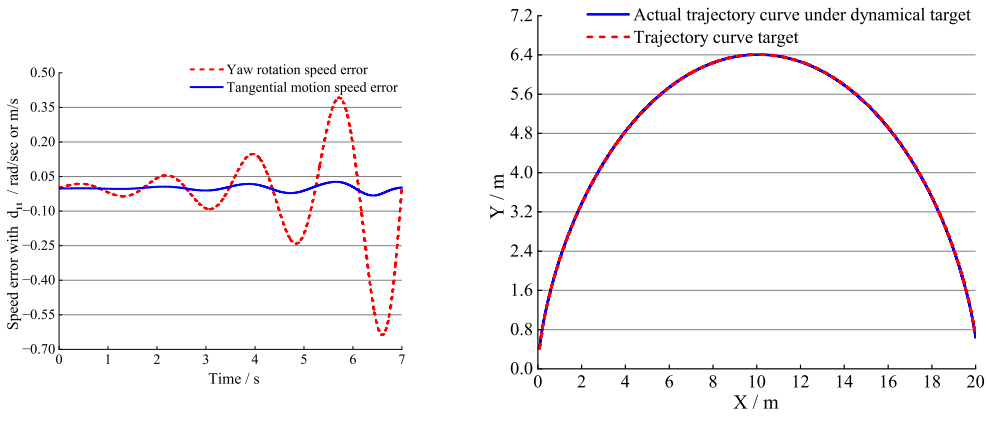
Figure 4. Actual motion speed errors and motion trajectory of the TWMR via the statical target. (**a**) Actual motion speed errors of the TWMR; (**b**) actual motion trajectory curve of the TWMR.

5.2. Accurate Trajectory Tracking with Unstable Speed Error Subsystems

In fact, although the speed error subsystems are unstable, actual motion trajectory can closely follow the prescribed path via dynamical tracking target. In what follows, two types of uncertain factors acting on the yaw motion speed error subsystem are explored to further verify the influence of uncertainties on path tracking.

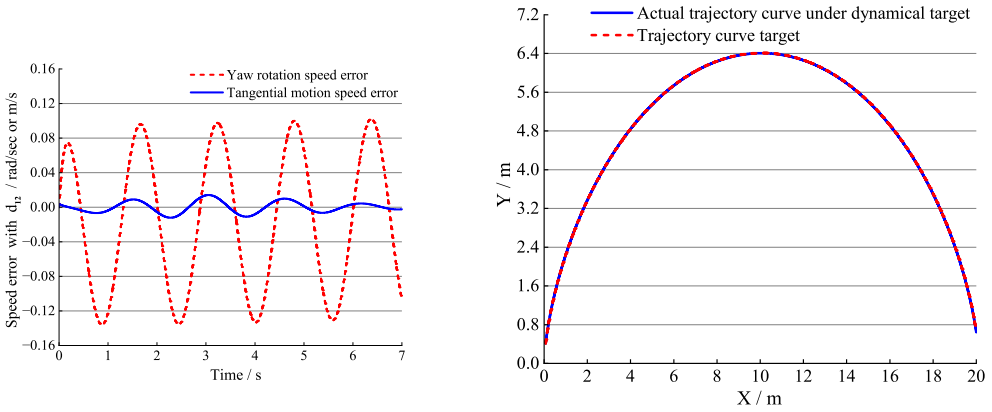
On the one hand, we denote the uncertainty as $\boldsymbol{d}_1 = \boldsymbol{d}_{11} = (12y_1,\ 11.2y_2)^{\mathrm{T}}$, which is an internal system uncertainty related to the error state. In this case, the yaw motion speed error subsystem becomes unstable when Equation (42) is applied. As shown in Figure 5, despite increasing speed errors, the actual motion trajectory can achieve satisfactory tracking performance if the tangential motion speed error remains sufficiently small. This implies that throughout the motion process, the actual location error remains manageable, and the speed error does not accumulate significantly due to the modified dynamic tracking target.

On the other hand, we choose the uncertainty as $\boldsymbol{d}_1 = \boldsymbol{d}_{12} = (\sin 4t,\ \cos 4t)^{\mathrm{T}}$, which represents an external disturbance independent of the error state. Figure 6a shows that both tangential speed error and yaw motion speed error are not convergent to zero. However, as shown in Figure 6b, the TWMR can still effectively follow the prescribed path if the tangential motion speed error remains sufficiently small. Moreover, the corresponding control inputs of the TWMR is decribed yin Figure 7a,b.



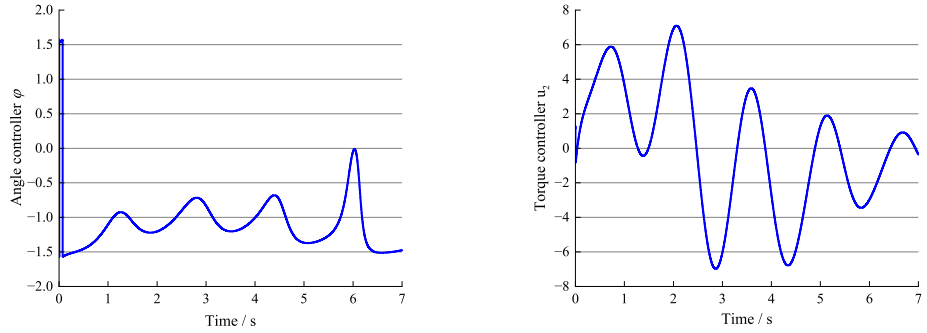
(**a**) (**b**)

Figure 5. Actual motion speed errors and motion trajectory of the TWMR under the internal uncertainty $\boldsymbol{d}_{11}$. (**a**) Actual motion speed errors of the TWMR; (**b**) Actual motion trajectory curve of the TWMR.



(**a**) (**b**)

Figure 6. Actual motion speed errors and motion trajectory of the TWMR under the external disturbance $\boldsymbol{d}_{12}$. (**a**) Actual motion speed errors of the TWMR; (**b**) Actual motion trajectory curve of the TWMR.



(**a**) (**b**)

Figure 7. Angle control input and torque control input of the TWMR under external disturbance $\boldsymbol{d}_{12}$. (**a**) Angle control input of the TWMR; (**b**) torque control input of the TWMR.

In the following, we calculate the square error between the actual motion trajectory and the target trajectory to validate the effects of uncertainties on trajectory tracking error.

Let $(x_a(k), y_a(k))$ denote a known point on the actual motion trajectory. For the same horizontal coordinate $x_a(k)$, we define $(x_a(k), \hat{y}_a(k))$ as the corresponding point on the target trajectory curve. Since $x_a(k)$ is known, according to Equation (46), we have

$$\begin{cases} x_a(k) = 3.2056 \cdot [t_k + 0.5121 - \sin(t_k + 0.5121)], \\ \hat{y}_a(k) = 3.2056 \cdot [1 - \cos(t_k + 0.5121)]), \end{cases} \tag{52}$$

in which case, $\hat{y}_a(k)$ can be calculated. Then, the square error between $(x_a(k), y_a(k))$ and $(x_a(k), \hat{y}_a(k))$ can be expressed by $(y_a(k) - \hat{y}_a(k))^2$. As a consequence, the sum of these errors is denoted as $J_a = \sum_{k=1}^{N} (y_a(k) - \hat{y}_a(k))^2$ with time step $h = 0.001$ and $N = \frac{20}{h}$. By calculating the trajectory tracking error in Figure 6b, we obtain $J_a = 6.3217$. Accordingly, the formula for calculating the average error per point is given by $\sqrt{\frac{J_a}{N}} = \sqrt{\frac{6.3217}{20000}} < 0.02$. Therefore, the quantitative results show that by applying the proposed control strategy the TWMR can track the target path accurately despite various uncertainties.

6. Conclusions

The nonholonomic constraints and motion laws of a TWMR are comprehensively elucidated in this paper. Compared to existing related research, our study exhibits two distinctive features. (i) In order to agree well with engineering practices, the steering

angle of the front wheel is considered as a control variable rather than a state variable. In this sense, the dynamic model becomes more complicated, and an intermediate control variable has to be introduced to determine the steering angle. (ii) By incorporating the relative curvature of a prescribed curve, a modified dynamical tracking target that matches well the dynamic model is constructed. On this basis, the original obstacle avoidance motion issue is transformed to a conventional tracking control problem. The core essence of the modified dynamic tracking target lies in the relative curvature, which significantly enhances trajectory tracking accuracy and robustness. Moreover, the yaw motion speed target can be chosen freely for better tracking performance in practical scenarios. Finally, simulation results indicate that trajectory deviation can be greatly reduced, even in the presence of unstable speed error subsystems.

The modified dynamical tracking target can be widely utilized to precisely track a given smooth trajectory curve for various nonholonomic mechanical structures such as robots, aircraft, and steamers. Moreover, the dynamical tracking target method can be further extended to a space trajectory curve by incorporating curve torsion, which is our future research.

Author Contributions: The authors X.W. and Y.Z. contributed equally to this work. All authors have read and agreed to the published version of the manuscript.

Funding: The work was supported by the National Natural Science Foundation under grant (12162006). Also, it was supported by Cultivation Project of Yibin University (2022PY31), and the Guizhou Provincial Science and Technology Projects (ZK[2023] 037, [2023]119).

Data Availability Statement: Data are contained within the article.

Conflicts of Interest: The authors declare no conflicts of interest.

Appendix A

Appendix A.1. The Detailed Derivation Process of the Dynamic Model

Since the system energy is mainly provided by the driven motors on the right and left rear wheels, all posture variables $(x, y, \theta)^{\mathrm{T}}$ are achieved by the coupling action of nonholonomic constraints. In what follows, we will calculate the system kinetic energy. As depicted in Figure 1, position relations between point O and the center points of the two rear wheels are described by

$$\begin{cases} x_{wl} = x + \frac{d}{2}\sin\theta, \\ y_{wl} = y - \frac{d}{2}\cos\theta, \end{cases} \qquad \begin{cases} x_{wr} = x - \frac{d}{2}\sin\theta, \\ y_{wr} = y + \frac{d}{2}\cos\theta. \end{cases} \tag{A1}$$

Here, (x_{wl}, y_{wl}) and (x_{wr}, y_{wr}) represent the coordinates of the center points of the left and right rear wheels, respectively. Similarly, position relations among points C, P, and O are given by

$$\begin{cases} x_C = x + \frac{a}{2}\cos\theta, \\ y_C = y + \frac{a}{2}\sin\theta, \end{cases} \qquad \begin{cases} x_P = x + a\cos\theta, \\ y_P = y + a\sin\theta. \end{cases} \tag{A2}$$

In the first place, the sum of the translational energy and rotational kinetic energy of the two rear wheels can be formulated as

$$\begin{aligned} T_w =& \frac{1}{2}M_w(v_{wl}^2 + v_{wr}^2) + \frac{1}{2}I_w(\dot{\theta}_r^2 + \dot{\theta}_l^2) + I_{wd}\dot{\theta}^2 \\ =& M_w(\dot{x}^2 + \dot{y}^2 + \frac{d^2}{4}\dot{\theta}^2) + \frac{1}{2}I_w(\dot{\theta}_r^2 + \dot{\theta}_l^2) + I_{wd}\dot{\theta}^2, \end{aligned} \tag{A3}$$

where v_{wr}, v_{wl} are the tangential motion speeds of the center points of the right and left rear wheels, respectively. Moreover, the sum of the translational energy and rotational kinetic energy of the center rod can be presented as

$$T_b = \frac{1}{2}M_b[\dot{x}^2 + \dot{y}^2 + \frac{a^2}{4}\dot{\theta}^2 - a\dot{\theta}(\dot{x}\sin\theta - \dot{y}\cos\theta)] + \frac{1}{2}I_b\dot{\theta}^2. \tag{A4}$$

Furthermore, the sum of the translational energy and rotational kinetic energy of the front wheel can be expressed as

$$T_f = \frac{1}{2}(M_w + \frac{I_w}{r^2})[\dot{x}^2 + \dot{y}^2 + a^2\dot{\theta}^2 - 2a\dot{\theta}(\dot{x}\sin\theta - \dot{y}\cos\theta)]. \tag{A5}$$

Therefore, the Lagrangian function is obtained by

$$L = T_w + T_b + T_f.$$

Substituting L into Equation (14), the dynamic equation is derived as

$$\boldsymbol{A}(\boldsymbol{q})\ddot{\boldsymbol{q}} + \boldsymbol{U}(\boldsymbol{q}, \dot{\boldsymbol{q}})\dot{\boldsymbol{q}} = \boldsymbol{E}(\boldsymbol{q})\boldsymbol{\tau} + \boldsymbol{F}^{\mathrm{T}}(\boldsymbol{q})\boldsymbol{\lambda} \tag{A6}$$

where

$$\begin{aligned} \boldsymbol{A}(\boldsymbol{q}) &= \begin{bmatrix} M_1 & 0 & -M_2 a\sin\theta & 0 & 0 \\ 0 & M_1 & M_2 a\cos\theta & 0 & 0 \\ -M_2 a\sin\theta & M_2 a\cos\theta & I & 0 & 0 \\ 0 & 0 & 0 & I_w & 0 \\ 0 & 0 & 0 & 0 & I_w \end{bmatrix}, \\ \boldsymbol{U}(\boldsymbol{q}, \dot{\boldsymbol{q}}) &= \begin{bmatrix} 0 & 0 & -M_2 a\dot{\theta}\cos\theta & 0 & 0 \\ 0 & 0 & -M_2 a\dot{\theta}\sin\theta & 0 & 0 \\ 0 & 0 & 0 & 0 & 0 \\ 0 & 0 & 0 & 0 & 0 \\ 0 & 0 & 0 & 0 & 0 \end{bmatrix}, \end{aligned} \tag{A7}$$

with $M_1 = M_b + 3M_w + \frac{1}{r^2}I_w$, $M_2 = \frac{1}{2}M_b + M_w + \frac{1}{r^2}I_w$, and $I = I_b + 2I_{wd} + \frac{a^2}{4}M_b + \frac{d^2}{2}M_w + a^2M_w + \frac{a^2}{r^2}I_w$. Taking the derivative of both sides of Equation (11) with respect to time and substituting it into Equation (A6) results in

$$\boldsymbol{A}(\boldsymbol{q})\boldsymbol{S}(\boldsymbol{q})\dot{\boldsymbol{V}} + \boldsymbol{A}(\boldsymbol{q})\dot{\boldsymbol{S}}(\boldsymbol{q})\boldsymbol{V} + \boldsymbol{U}(\boldsymbol{q}, \dot{\boldsymbol{q}})\boldsymbol{S}(\boldsymbol{q})\boldsymbol{V} = \boldsymbol{E}(\boldsymbol{q})\boldsymbol{\tau} + \boldsymbol{F}^{\mathrm{T}}(\boldsymbol{q})\boldsymbol{\lambda}. \tag{A8}$$

Multiplying Equation (A8) by $\boldsymbol{S}^{\mathrm{T}}(\boldsymbol{q})$ from the left, and together with Equation (13), yields

$$(\boldsymbol{S}^{\mathrm{T}}(\boldsymbol{q})\boldsymbol{A}(\boldsymbol{q})\dot{\boldsymbol{S}}(\boldsymbol{q}) + \boldsymbol{S}^{\mathrm{T}}(\boldsymbol{q})\boldsymbol{U}(\boldsymbol{q}, \dot{\boldsymbol{q}})\boldsymbol{S}(\boldsymbol{q}))\boldsymbol{V} + \boldsymbol{S}^{\mathrm{T}}(\boldsymbol{q})\boldsymbol{A}(\boldsymbol{q})\boldsymbol{S}(\boldsymbol{q})\dot{\boldsymbol{V}} = \boldsymbol{S}^{\mathrm{T}}(\boldsymbol{q})\boldsymbol{E}(\boldsymbol{q})\boldsymbol{\tau}. \tag{A9}$$

After being further calculated, the dynamic Equation (A9) is rewritten in a state equation form as

$$\begin{cases} \dot{v} = -\frac{Iar^2\dot{\varphi}\sin\varphi}{\Delta\cos\varphi}v + \frac{ra^2\cos^2\varphi}{\Delta}u_2, \\ \ddot{\theta} = \dot{\omega} = cu_1, \end{cases} \tag{A10}$$

where $\Delta = M_1a^2r^2\cos^2\varphi + 2I_wa^2\cos^2\varphi + Ir^2\sin^2\varphi$, $c = \frac{r}{dI_w}$, $u_1 = T_l - T_r$, $u_2 = T_l + T_r$.

References

1. Guo, F.; Yang, H.; Wu, X. Model-based deep learning for low-cost IMU dead reckoning of wheeled mobile robot. *IEEE Trans. Ind. Electron.* **2023**, *1* , 7531–7541. [CrossRef]
2. Zhao, L.; Li, J.; Li, H. Double-loop tracking control for a wheeled mobile robot with unmodeled dynamics along right angle roads. *ISA Trans.* **2023**, *136*, 525–534. [CrossRef] [PubMed]
3. Parhi, D.R.; Deepak, B. Kinematic model of three wheeled mobile robot Journal of Mechanical Engineering Research. *J. Mech. Eng. Res.* **2011**, *3*, 307–318.
4. He, W.; Li, Z.J.; Chen, C.L.P. A survey of human-centered intelligent robots: Issues and challenges. *IEEE-CAA J. Autom. Sin.* **2017**, *4*, 602–609. [CrossRef]
5. Lin, H.Y.; Tsai, S.H.; Chen, K.Y. Design and implementation of the trajectory tracking and dynamic obstacle avoidance of wheeled mobile robot based on T-S fuzzy model. *Int. J. Fuzzy Syst.* **2023**, *25*, 2423–2438. [CrossRef]
6. Saenz, A.; Santibañez, V.; Bugarin, E. Velocity control of an omnidirectional wheeled mobile robot using computed voltage control with visual feedback: Experimental results. *Int. J. Control. Autom. Syst.* **2021**, *19*, 1089–1102. [CrossRef]
7. Savaee, E.; Rahmani Hanzaki, A. A new algorithm for calibration of an omni-directional wheeled mobile robot based on effective kinematic parameters estimation. *J. Intell. Robot. Syst.* **2021**, *101*, 28. [CrossRef]

8. Huang, J.; Chen, J.; Fang, H. An overview of recent progress in high-order nonholonomic chained system control and distributed coordination. *J. Control. Decis.* **2015**, *2*, 64–85. [CrossRef]
9. Li, H.P.; Yan, W.S.; Shi, Y. A receding horizon stabilization approach to constrained nonholonomic systems in power form. *Syst. Control. Lett.* **2017**, *99*, 47–56. [CrossRef]
10. Korayem, M.H.; Shafei, A.M. Motion equation of nonholonomic wheeled mobile robotic manipulator with revolute-prismatic joints using recursive gibbs-appell formulation. *Appl. Math. Model.* **2015**, *39*, 1701–1716. [CrossRef]
11. Kaliński, K.J.; Buchholz, C. Mechatronic design of strongly nonlinear systems on a basis of three wheeled mobile platform. *Mech. Syst. Signal Process.* **2015**, *52-53*, 700–721. [CrossRef]
12. Garcia-Sánchez, J.R.; Tavera-Mosqueda, S.; Silva-Ortigoza, R.; Hernández-Guzmán, V.M. A novel dynamic three-level tracking controller for mobile robots considering actuators and power stage subsystems: Experimental assessment. *Sensors* **2020**, *17*, 49–59. [CrossRef]
13. Silva-Ortigoza, J.R. Garcia-Sánchez, R.; Hernández-Guzmán, V.M.; Marquez-Sanchez, C. Trajectory tracking control for a differential drive wheeled mobile robot considering the dynamics related to the actuators and power stag. *IEEE Lat. Am. Trans.* **2016**, *14*, 657–664. [CrossRef]
14. Zheng, Y.J.; Zheng, J.C.; Shao, K.; Zhao, H.; Man, Z.H.; Sun, Z. Adaptive fuzzy sliding mode control of uncertain nonholonomic wheeled mobile robot with external disturbance and actuator saturation. *Inf. Sci.* **2024**, *663*, 120303. [CrossRef]
15. Airton, D.S.; Frank, S. A robotic walker based on a two-wheeled inverted pendulum. *J. Intell. Robot. Syst.* **2017**, *86*, 17–34.
16. Guo, Z.Q.; Xu, J.X.; Lee, T.H. Design and implementation of a new sliding mode controller on an underactuated wheeled inverted pendulum. *J. Frankl. Inst.* **2014**, *351*, 2261–2282. [CrossRef]
17. Furuichi, H.; Huang, J.; Fukuda, T.; Matsuno, T. Switching dynamic modeling and driving stability analysis of three-wheeled narrow tilting vehicle. *IEEE-ASME Trans. Mechatronics* **2014**, *19*, 1309–1322. [CrossRef]
18. Chatterjee, M.; Kale, M.; Chaudhari, B. A dynamic stability control for electric narrow tilting three wheeled vehicle using integrated multivariable controller. *Transp. Res. Part Transp. Environ.* **2019**, *66*, 58–75. [CrossRef]
19. Hacene, N.; Mendil, B. Fuzzy behavior-based control of three wheeled omnidirectional mobile robot. *Int. J. Autom. Comput.* **2019**, *16*, 163–185. [CrossRef]
20. Viet, T.D.; Doan, P.T.; Hung, N. Tracking control of a three-wheeled omnidirectional mobile manipulator system with disturbance and friction. *J. Mech. Sci. Technol.* **2012**, *26*, 2197–2211. [CrossRef]
21. Guo, Y.J.; Yu, L.; Xu, J.M. Robust finite-time trajectory tracking control of wheeled mobile robots with parametric uncertainties and disturbances. *J. Syst. Sci. Complex.* **2019**, *32*, 1358–1374. [CrossRef]
22. Yang, H.J.; Wang, S.Z.; Zuo, Z.Q.; Li, P. Trajectory tracking for a wheeled mobile robot with an omnidirectional wheel on uneven ground. *IET Control. Theory Appl.* **2020**, *14*, 921–929. [CrossRef]
23. Zhou, Y.S.; Wang, Z.H. Motion controller design of wheeled inverted pendulum with an input delay via optimal control theory. *J. Optim. Theory Appl.* **2016**, *168*, 625–645. [CrossRef]
24. Zhou, Y.S.; Wang, Z.H.; Chung, K.K. Turning motion control design of a two-wheeled inverted pendulum using curvature tracking and optimal control. *J. Optim. Theory Appl.* **2019**, *181*, 634–652. [CrossRef]
25. Zhou, Y.S.; Wang, Z.H. Robust motion control of a two-wheeled inverted pendulum with an input delay based on optimal integral sliding mode manifold. *Nonlinear Dyn.* **2016**, *85*, 2065–2074. [CrossRef]
26. Mobayen, S. Chaos synchronization of uncertain chaotic systems using composite nonlinear feedback based integral sliding mode control. *ISA Trans.* **2018**, *77*, 100–111. [CrossRef]

Disclaimer/Publisher's Note: The statements, opinions and data contained in all publications are solely those of the individual author(s) and contributor(s) and not of MDPI and/or the editor(s). MDPI and/or the editor(s) disclaim responsibility for any injury to people or property resulting from any ideas, methods, instructions or products referred to in the content.